energy&fuels

pubs.acs.org/EF Article

Influence of Catalyst Acidity on the Hydrogenation and Dimerization of Conjugated Olefins over Supported NiMoS Catalysts

Majed A. Alamoudi, Hamad Almohamadi, and Kevin J. Smith*

Cite This: *Energy Fuels* 2021, 35, 10113−10121 Read Online

ACCESS | Metrics & More | Article Recommendations | Supporting Information

ABSTRACT: The hydrogenation and dimerization of isoprene and 4-methylstyrene over supported NiMoS catalysts have been studied under conditions relevant to the hydrogenation of Canadian oil sands naphtha, during which the undesired dimerization of conjugated olefins, present in naphtha, is known to occur. NiMoS was dispersed on SiO_2−Al_2O_3 supports with varying Si/Al contents to determine the impact of the catalyst acidity on the dimerization reactions. The reactions were carried out in a microscale trickle-bed reactor operated at 200−250 °C, 3.4 MPa H_2, and liquid hourly space velocity (LHSV) of 2−4 h^{-1} for reaction periods of 3 days of continuous operation. The acidity of the NiMoS/Al_2O_3 catalyst, measured by NH_3 temperature-programmed desorption and pyridine adsorption diffuse reflectance infrared Fourier transform spectroscopy, was lower than that of the NiMoS/SiO_2−Al_2O_3 catalysts, which increased with increased SiO_2 content up to 20 wt % SiO_2. The results showed that dimer formation correlated with the acidity of the catalysts. The dimer yield on the sulfided supports without NiMoS was about 40% of the yield observed on the NiMoS/SiO_2−Al_2O_3 catalysts. The NiMoS catalysts showed stable activity over 3 days of continuous operation, whereas the sulfided supports deactivated rapidly because of low hydrogenation activity. Addition of 3 wt % NaOH to the NiMoS/S10 catalyst neutralized 60% of the acid sites, resulting in a 50% drop in dimerization yield.

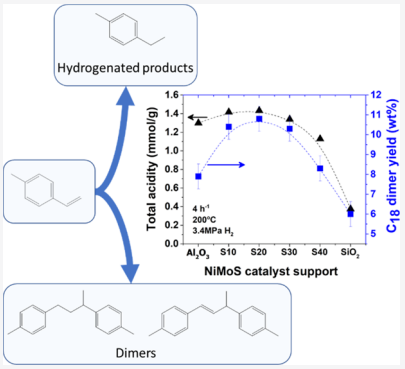

Downloaded via UNIV OF BRITISH COLUMBIA on May 11, 2022 at 17:42:35 (UTC).
See https://pubs.acs.org/sharingguidelines for options on how to legitimately share published articles.

INTRODUCTION

Canada has 167.7 billion barrels (2019) or ∼10.5% of the world's proven oil reserves.[1] Production from the Canadian oil sands reached 2.29 million barrels/day in 2015 and is expected to increase to 4 million barrels/day by 2024. The oil sands occur as a natural mixture of 9−13% bitumen, 3−7% water, and 80−85% sand.[2] To obtain valuable products, bitumen is first extracted from the oil sands before primary upgrading, either by carbon rejection or hydrogen addition, to increase the H/C ratio of the oil. Finally, heteroatoms (S, N, and metals) are removed by hydrotreating to obtain a synthetic sweet crude oil product.[3]

There are two different types of coker technology used in upgrading oil sands: delayed cokers and fluid cokers. Both cokers yield light gas oil, naphtha, middle distillate, and heavy gas oil products with different product yields. The products contain significant quantities of heteroatoms (Table S1) that must be removed in subsequent hydrotreating steps.[4] However, naphtha (and light gas oil) contains high amounts of olefins (∼20 wt %) and diolefins (∼4.4 wt %),[5] which are known to dimerize under hydrotreating reaction conditions, producing gums that deposit on the catalyst, causing catalyst deactivation, increased reactor fouling, and eventual reactor shutdown.[5] Hence, prior to passing coker naphtha to a naphtha hydrotreater, a mild hydrogenation (<250 °C), aimed at saturating the olefins and diolefins, is performed. However, even though the hydrogenation is done at a mild temperature, catalyst deactivation and reactor fouling may still occur.[5]

Several types of catalysts have been used for hydrogenation processes, including metal sulfides (Co, Mo, Ni, and W) and noble metals (Ru, Pd, Cu, Ir, and Pt).[6−10] Ni−Mo−S and Co−Mo−S are most commonly used for crude oil hydrogenation because of their ability to resist poisoning by S- and N-containing heteroaromatics. The heteroaromatics must be removed to produce ultralow S fuels that satisfy the <10 ppm S requirement of Directive 2009/30/EC of the Council of the European Parliament.[11] Numerous studies have reported on olefin hydrogenation over MoS_2 catalysts,[10,12−14] but most of them were conducted at high temperatures (>250 °C) and high H_2 pressure >3.4 MPa, aiming at the removal of either N or S while minimizing aromatic hydrogenation and hydrogenolysis to maintain the fuel value of the feed.[10,12−14] Few studies of olefin and diolefin hydrogenation on MoS_2 under mild operating conditions (<250 °C and ∼3.4 MPa) have been reported.[12−14] One study by Alzaid et al.[15] examined both

Received: March 12, 2021
Revised: May 18, 2021
Published: June 8, 2021

© 2021 American Chemical Society

https://doi.org/10.1021/acs.energyfuels.1c00787
Energy Fuels 2021, 35, 10113−10121

olefin/diolefin hydrogenation and dimerization reactions and their kinetics over a commercial Ni−Mo−S/γ-Al_2O_3 catalyst under industrial reaction conditions: < 250 °C, 3.4 MPa H_2 pressure, 1−2 h^{-1} liquid hourly space velocity (LHSV), and a constant H_2/feed ratio of 392 mL(STP)/mL using model olefin/diolefin reactants in decalin. Alzaid et al.[16] reported that hydrogenation and dimerization occurred as simultaneous reactions, and at conditions corresponding to low hydrogenation activity, the dimerization yield increased significantly. Dimerization correlated with oligomerization and gum formation, which resulted in significant catalyst deactivation and increased pressure drop across the catalytic fixed-bed. The authors hypothesized that the catalyst Brønsted acidity was the cause of dimerization, without identifying the source or quantity of Brønsted acid sites.[16]

Past studies have also reported that the formation of gum/coke initially involves the formation of precursors on supported metal sulfide catalysts, for instance, by the dimerization of olefins, diolefins, and aromatics on the acidic sites of the catalyst.[17−19] The acid sites can donate a proton to another olefin/diolefin, forming an intermediate carbenium ion needed for the formation of dimers (and oligomers). Coke formation can also result from the hydrocarbon pyrolysis or dehydrogenation of heavy hydrocarbons, which leads to the formation of carbon and occurs at elevated temperatures >500 °C. On the other hand, gum formation that results from oligomerization reactions on acid sites generally does not occur at temperatures exceeding 300 °C.[20,21]

Weissman and Edwards[22] focused their studies on the deactivation of hydrotreating NiMoS and CoMoS catalysts supported on alumina. They simulated industrial reaction conditions by operating at 280−390 °C, 5.5 MPa, LHSV = 2 h^{-1}, and a H_2/feed ratio of 360 cm^3(STP)/cm^3 using naphtha and gas oil as feeds. The authors reported that catalyst deactivation was mostly because of the low-density carbon deposition on the catalyst, which blocked the active sites. In another study of catalyst deactivation by Alzaid et al.,[16] the hydrogenation of the conjugated olefins α-methylstyrene and 4-methylstyrene (4-MS) was compared over a continuous time-on-stream (TOS) reaction period of 30 days using a commercial NiMoS/γ-Al_2O_3 catalyst. The authors reported significant gum formation and increased pressure drop across the reactor with an increased TOS when 4-MS was the reactant, but negligible pressure drop occurred when using α-methylstyrene.[16] The study illustrated the impact of molecular structure on dimerization, with the vinyl group of α-methylstyrene sterically hindered by the methyl group, resulting in the low yield of dimers. The study also demonstrated that olefin dimerization correlated with gum formation and high gum yield correlated with high pressure drop, catalyst deactivation, and reactor fouling.

Dimerization is a chemical process that links monomeric compounds, and dimerization of olefins on acid catalysts is well known.[23−25] Dimerization is also known to occur on MoS_2 catalysts used in hydrotreating reactions.[10,13,14,26] Wambeke et al.[13] studied the hydrogenation of isoprene over MoS_2/γ-Al_2O_3 and reported that the active sites for hydrogenation were the three coordinately unsaturated sites (CUS) of Mo atoms on the edge of the $(\bar{1}010)$ plane of the MoS_2 slab. These active sites have three vacancies and one unsaturated S atom. Jalowiecki et al.[14] confirmed the results obtained by Wambeke et al.[13] for isoprene hydrogenation over unsupported MoS_2. They also reported that the active sites for *cis*-1,3-pentadiene isomerization were the two and four CUS atoms on the edge of the $(\bar{1}010)$ plane of the MoS_2 slab. In relation to this study, Okuhara et al.[10] observed that the isomerization reaction occurs via a carbocation mechanism on the S layer of the MoS_2 crystal. An active proton on the S layer catalyzes the formation of a tertiary carbocation intermediate from 2-methyl-1-butene that is therefore converted to 2-methyl-2-butene. Yang and Satterfield[26] proposed that the dissociative adsorption of H_2S on Ni−Mo−S/γ-Al_2O_3 can form a Brønsted acid site by converting a S vacancy to a −SH group. The authors also reported that another source of Brønsted acid sites could result from the addition of a P_2O_5 promoter that is commonly present in Ni−Mo−S/γ-Al_2O_3 commercial catalysts. These findings are the subject of interest for the current study as they assume the existence of Brønsted acid sites which have the ability to protonate a diolefin that leads to the formation of an allylic carbocation, the intermediate for dimer formation. Yang and Satterfield[26] confirmed the presence of Brønsted acid sites, but they could not distinguish between the acid sites generated by H_2S or P_2O_5 promoters.

Pérez-Martínez et al.[25] investigated amorphous aluminosilicates (ASA) with different Si/(Si + Al) ratios as supports of CoMoS catalysts in the hydrotreating of synthetic fluid catalytic cracking naphtha. The feed (2 wt % of 2-methlythiophene and a 20 wt % mixture of 2,4,4-trimethyl-1-pentene and 2,4,4-trimethyl-2-penten in *n*-heptane) was reacted at 17 MPa, 523 K, 20 mL/h liquid flow rate, and a H_2/liquid feed ratio of 500. They reported that the catalyst acidity increased with an increase in the Si/(Si + Al) ratio and showed a maximum at approximately 50% Si/(Si + Al). They also noted that while the Si/(Si + Al) ratio increased, the activity of the acid-catalyzed reactions increased (alkylation, isomerization, and cracking) and hydrodesulfurization and olefin hydrogenation (HYDO) decreased. According to the literature, stronger Brønsted acid sites are required for alkylation and cracking while weaker Brønsted acid sites are needed for isomerization reactions.[27] The authors also indicated that a small amount of oligomers was formed (1 wt % of the products) at the conditions tested.

Among the aforementioned studies, the source of the acidity that causes dimerization at industrially relevant conditions, particularly at the relatively low temperature used for the hydrogenation of Canadian oil sands naphtha, has not been identified. Herein, we report on the effect of support acidity on the yield of dimerization products over a series of NiMoS catalysts and hence identify the main source of the acidity for the dimerization (oligomerization) reactions at conditions relevant to the hydrogenation of Canadian oil sands naphtha.

EXPERIMENTAL SECTION

A series of commercial SiO_2−Al_2O_3 supports, with varying Si/Al ratios (Siral 10, 20, 30, 40, mesh no. 230−270, SASOL, Germany GmbH, with 10, 20, 30, and 40 wt % SiO_2, respectively), a silica gel (silica gel, technical grade 40, 6−14 mesh, Sigma-Aldrich), and Al_2O_3 (mesh no. 8−12, SASOL, Germany GmbH) were used as supports of NiMoS. To limit the effects of internal and external mass transfer, the catalyst particle size was maintained below 1.41 mm.[28] In the case of Siral powders, particles were formed by extrusion after adding boehmite (AlOOH) (SASOL, Germany, GmbH) as a particle binder. Approximately 70 wt % distilled water, 10 wt % HNO_3 as peptizing agent, 4 wt % boehmite, and 16 wt % of the Siral powder were mixed together to form a paste for extrusion. The supports were calcined at 700 °C for 2 h in air before sieving to the appropriate particle size. These supports are referenced herein as Al_2O_3, SiO_2, S10, S20, S30,

https://doi.org/10.1021/acs.energyfuels.1c00787
Energy Fuels 2021, 35, 10113−10121

Table 1. Textural Properties and Acidities of the Different Supports and NiMoS Catalysts

					acidity			
sample	SiO_2 content wt %	BET area[a] m2/g	pore volume cm3/g	pore size nm	total[b] mmol/g	Lewis[c] mmol/g	Brønsted[c] mmol/g	B:L
Al_2O_3	0	225	0.55	10	0.643			
Al_2O_3−S	0	257	0.58	8.9	1.024			
NiMoS/Al_2O_3	0	222	0.41	7.6	1.300	1.15	0.15	0.13
S10	10	330	0.63	8.0	0.774			
S10−S	10	324	0.61	7.6	1.019			
NiMoS/S10	10	244	0.42	7.0	1.417	1.25	0.17	0.14
S20	20	313	0.65	8.0	0.704			
S20−S	20	285	0.61	8.6	1.041			
NiMoS/S20	20	227	0.46	8.1	1.433	1.25	0.18	0.15
S30	30	412	0.8	8.0	0.633			
S30−S	30	386	0.76	7.9	1.059			
NiMoS/S30	30	245	0.53	8.6	1.340	1.23	0.11	0.09
S40	40	406	0.88	9.0	0.500			
S40−S	40	357	0.83	9.3	0.867			
NiMoS/S40	40	265	0.65	9.8	1.129	1.08	0.05	0.04
SiO_2	100	502	0.32	2.5	0.093			
SiO2−S	100	464	0.3	2.6	0.189			
NiMoS/SiO_2	100	376	0.27	2.9	0.375	0.38		0.38

[a]Measured by BET N_2 adsorption. [b]Measured by TPD of NH_3. [c]Measured by Py-DRIFT.

and S40, where SXX identifies the original Siral support, with XX denoting the wt % of SiO_2.

Ni−Mo was subsequently added to the supports by incipient wetness impregnation to obtain a Mo loading of ∼8 wt % and a Ni loading of ∼2 wt %.[16] To overcome solubility issues, multiple impregnations from a 0.4 g Mo/cm^3 aqueous solution of $(NH_4)_6Mo_7O_{24}{\cdot}4H_2O$ (Sigma-Aldrich, 81.0−83.0% MoO_3 basis) and a 0.2 g Ni/cm^3 solution of $Ni(OCOCH_3)_2{\cdot}4H_2O$ (99.998% trace metal basis, Sigma-Aldrich) were implemented as required. After each impregnation, the sample was aged overnight and dried at 100 °C for 2 h, followed by calcination at 450 °C for 4 h.

Prior to the activity tests, both the supports and the supported NiMoS catalysts were presulfided ex situ in a microscale trickle-bed reactor (length 50 cm; hot zone 30 cm) with an internal diameter of 1.18 cm using 6 g catalyst, 391.5 g decalin, and 8.5 g CS_2 at 300 °C, LHSV 2 h^{-1}, H_2/feed ratio of 392 mL (STP)/mL, and 3.4 MPa H_2 for 8 h to yield the sulfided supports Al_2O_3−S, SiO_2−S, S10−S, S20−S, S30−S, S40−S and the sulfided catalysts NiMoS/Al_2O_3, NiMoS/SiO_2, NiMoS/S10, NiMoS/S20, NiMoS/S30, and NiMoS/S40. ICP-OES was used to confirm that the NiMoS loading on Al_2O_3 was 8.34 wt % Mo and 2.21 wt % Ni.

The total Brunauer−Emmett−Teller (BET) surface area, average pore width, and pore volume of the prepared catalysts were determined from N_2 adsorption−desorption isotherms measured at 77 K using a Micrometrics accelerated surface area and porosimetry (ASAP 2020) analyzer. Prior to the analysis, the samples were degassed at 200 °C for 4 h under a vacuum pressure of 40 Pa to eliminate the adsorbed moisture. Repeat analyses showed an average error of ±5% in the BET area.

A Micromeritics Autochem II 2920 analyzer was used to determine the total acidity by NH_3 temperature-programmed desorption (NH_3 TPD). The samples (∼150 mg) were first dried in He at 200 °C for 2 h before cooling under He flow to 70 °C. NH_3 adsorption followed, flowing a 15% NH_3 in He mixture over the samples at 40 mL(STP)/min and 70 °C. After flushing the sample in He, the NH_3 desorption was then monitored using a thermal conductivity detector as the sample temperature was increased from 120 to 550 °C at 10 °C/min. The sample was held at the final temperature until no further NH_3 was detected in the effluent. Repeat analyses indicated an average error of ±5% in the total acidity measured for each sample.

Pyridine adsorption diffuse reflectance infrared Fourier transform (Py-DRIFT) spectroscopy was performed using a Thermo Nicolet 4700 FT-IR spectrometer equipped with a mercury cadmium telluride detector and an in situ DRIFT cell (Thermo Fisher Scientific, model no. 0030-102, serial no. 0904-004) to distinguish Lewis and Brønsted acid sites. The powdered sample was placed in the DRIFT cell and purged with N_2 at room temperature for 30 min, followed by heating to 400 °C for 2 h. After cooling to 200 °C, a background spectrum was collected. Pyridine vapor was then introduced to the sample for 10 min at 100 °C, followed by purging the cell for 30 min in N_2 flow as the cell temperature was increased to 200 °C, before recording the spectra of adsorbed pyridine.

Catalyst morphology was determined by HRTEM analysis (200 kV FEI Tecnai Osiris at a resolution limit of 0.14 nm). The catalysts were crushed and dispersed in isopropanol by sonication for 3−5 min. A drop of the prepared suspension was placed on a 300-mesh lacey carbon film with a Cu grid. From several representative micrographs, the length (L_i) and number of layers (N_i) of at least 200 MoS_2 crystallites were determined. The length of the crystallites (L_i) was used to estimate the number of edge-site Mo atoms (n_i) of a single layer, using the equation $L_i = 3.2(2n_i - 1)$ Å, assuming that the MoS_2 layers formed a perfect hexagon.[29] The MoS_2 dispersion, f_{Mo}, was then estimated using the following equation[30−32]

$$f_{Mo} = \frac{\sum_{i=1,..,x} 6n_i - 6}{\sum_{i=1,..,x} 3n_i^2 - 3n_i + 1}$$

where x is the total number of crystallites observed in the micrographs.

The hydrogenation reactions were conducted in a microscale, trickle-bed reactor (length, 50 cm; hot zone, 30 cm) with an internal diameter of 1.18 cm. The catalyst bed was prepared as described previously to ensure a uniform liquid flow through the bed.[16] Initially, some experiments were conducted using 2.4 wt % isoprene in decalin at 250 °C, 3.4 MPa H_2, LHSV 2 h^{-1}, H_2/feed ratio of 392 mL(STP)/mL, and a TOS period of 3 days. Another set of experiments was conducted using 8.4 wt % 4-MS in decalin at 200 °C, 3.4 MPa H_2, LHSV of 4 h^{-1}, and a H_2/feed ratio of 392 mL(STP)/mL for a TOS period of 3 days. The liquid product was collected every 24 h from a condenser placed after the reactor and held at room temperature. The gas flowed from the condenser to a scrubber containing NaOH (1 M) to remove H_2S prior to being vented. In order to quantify and identify the chemical components, the liquid product was analyzed using a Shimadzu QP-2010S gas chromatography−mass spectrometry (GC−MS) analyzer and a Shimadzu RXI-5MS column (internal diameter, 0.25 mm; length, 30 m; and film thickness, 0.25 μm). The reactant

https://doi.org/10.1021/acs.energyfuels.1c00787
Energy Fuels 2021, 35, 10113−10121

conversion (X), product selectivity (S), and yield (Y) were determined from the GC analysis as follows

$$A \rightarrow B + C$$

$$X_A = 1 - \frac{C_{W(A)}}{C_{W(A_0)}} = \frac{C_{W(B)} + C_{W(C)}}{C_{W(A)} + C_{W(B)} + C_{W(C)}}$$

$$S_B = \frac{C_{W(B)}}{C_{W(B)} + C_{W(C)}}$$

$$Y_B = \frac{C_{W(B)}}{C_{W(A)} + C_{W(B)} + C_{W(C)}}$$

where A represents the reactants, B represents the hydrogenation products, and C represents the dimerization products. $C_{W(j)}$ is the concentration of component j in the liquid product (wt %) and $C_{W(j0)}$ is the concentration of component j in the liquid feed (wt %). A balance placed under the feed flask was used to measure the mass of liquid delivered to the reactor and hence determine the overall mass balance using the following equation

$$\text{overall mass balance \%} = \left[\frac{\text{recovered product mass}}{\text{feed mass (4-MS + decalin)}}\right] \times 100$$

For all the experimental results reported herein, the overall mass balance closure was >92%. Excluding the solvent decalin, the mass balance was >85%. In addition, the overall experimental error estimated from a series of repeat experiments showed the absolute error in the product yields was ±1% (absolute percentage points). Calculation of the Mears criterion and the Weisz−Prater criterion confirmed that the yield data reported herein were free of external and internal mass transfer effects.[28]

RESULTS AND DISCUSSION

Table 1 reports the textural properties of the Si/Al supports, the same supports after ex situ sulfidation (designated as SXX−S), and the sulfided NiMoS/SiO_2−Al_2O_3 catalysts. The supports were all mesoporous, although the SiO_2 support had a much smaller average pore diameter (2.5 nm). After Ni + Mo addition to Al_2O_3 and following sulfidation, the surface area of the resulting NiMoS/Al_2O_3 catalyst was almost unchanged from that of Al_2O_3. In contrast, the surface area of the SiO_2 support decreased by 25% after the metal addition. The smaller pores of SiO_2 (2.5 nm), compared to that of Al_2O_3 (10 nm), likely resulted in some pore blocking after metal addition by impregnation. The properties of the Siral supports varied according to the relative amounts of SiO_2 in the support material, with the surface area of the NiMoS/SiO_2−Al_2O_3 catalysts decreasing as the SiO_2 content increased.

The catalyst acidities (NH_3 TPD profiles provided in Figures S1 and S2, Supporting Information) were also dependent on the SiO_2 content, as shown in Table 1. The sulfided supports had similar acidities except for S40−S and SiO_2−S, which showed significantly lower acidities. In the case of the supported catalysts, NiMoS/SiO_2 also had the lowest acidity among all the catalysts. Daniell et al.[33] reported that among the Siral supports calcined at 550 °C for 3 h, Siral 40 was the most acidic. The data of Table 1 indicate that Siral 10 and Siral 20 are the most acidic of the supports of the present study, but note that these samples were mixed with boehmite prior to calcination at 700 °C for 2 h. Lenarda et al.[34] have shown that the acidity of silica−aluminates decreases with increased calcination temperature and is dependent upon their composition.

The type of acidity of the catalysts was also dependent on the SiO_2 content, as shown in Table 1 and Figure S3 (Supporting Information). Brønsted acidity was maximum for the NiMoS/S20 catalyst, whereas it was not detectable on the NiMoS/SiO_2 catalyst. Lewis acidity did not show a clear trend among the catalysts, but NiMoS/SiO_2 had the lowest Lewis acidity.

High-resolution transmission electron microscopy (HRTEM, Figure S4 of Supporting Information) was used to estimate MoS_2 dispersion of the sulfided catalysts. As shown in Table 2, the MoS_2 dispersion was relatively constant for the Al_2O_3 and SiO_2−Al_2O_3 supports but decreased marginally on the SiO_2 support. However, the change in dispersion was low compared to the corresponding change in catalyst acidities, as reported in Table 1. Consequently, the changes in conversion and product selectivity that are reported with the variation in the SiO_2 content of the support can mostly be attributed to the catalyst acidities rather than the NiMoS dispersion.

Table 2. HRTEM Results for NiMoS Catalysts on Different Supports

	catalysts		
	NiMoS/Al_2O_3	NiMoS/S10	NiMoS/SiO_2
average number of MoS_2 layers, N	2.5 ± 1.3	2.6 ± 1.3	3.3 ± 1.2
average length, L (nm)	3.5 ± 1.4	3.7 ± 1.5	4.0 ± 2.3
average number of Mo edge sites	5.9	6.2	6.8
dispersion, f_{Mo}	0.28 ± 0.02	0.27 ± 0.03	0.25 ± 0.06

Figure 1 reports the catalyst acidity and the yield of dimers as a function of the catalyst support of the sulfided catalysts,

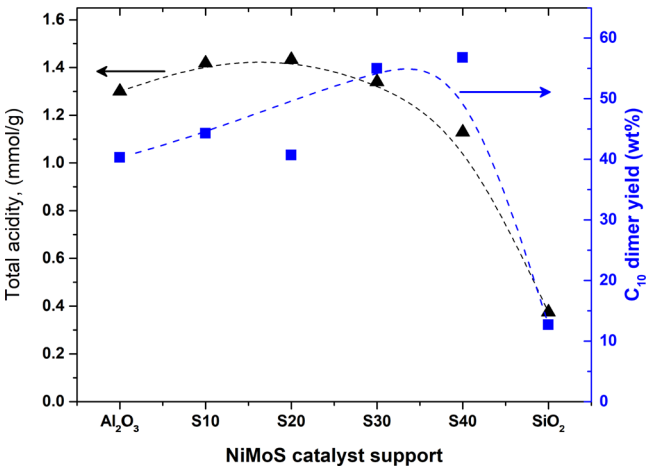

Figure 1. C_{10} yield related to the acidity of NiMoS catalysts on different supports measured at 250 °C, 3.4 MPa H_2, LHSV = 2 h^{-1}, H_2/feed = 392 mL(STP)/mL with 2.9 wt % isoprene in decalin, and TOS period of 3 days (dotted line to guide the eye).

when reacting 2.4 wt % isoprene in decalin at 250 °C, 3.4 MPa H_2, LHSV 2 h^{-1}, and H_2/feed ratio of 392 mL (STP)/mL, after a TOS period of 3 days. The NiMoS/SiO_2 catalyst had a significantly lower yield of C_{10} dimers and a lower acidity compared to the Siral-supported catalysts. Among these latter catalysts, no clear trend in dimerization yield was observed. However, isoprene was very reactive over all the catalysts with

https://doi.org/10.1021/acs.energyfuels.1c00787
Energy Fuels 2021, 35, 10113−10121

~100% conversion, even at less severe operating conditions.[28] Consequently, further studies focused on 4-MS as the reactant.

Table S2 presents the conversion and product yields for the NiMoS/S10 catalyst used to hydrogenate 8.4 wt % 4-MS in decalin at 200 °C, 3.4 MPa H_2, LHSV = 4 h^{-1}, and H_2/feed ratio of 392 mL(STP)/mL, over a TOS period of 3 days. The data show that 4-MS was mostly hydrogenated to 1-ethyl-4-methyl-benzene (yield >84 wt %) and C_{18} dimers. The hydrogenated product yield decreased slightly over the 3 day period from 88.7 to 84.1 wt %. The C_{18} dimer with the highest yield (9.7 wt %) was 1,3-di-(4′-methylphenyl) butane, and the total yield of all C_{18} dimers was 10.4 wt % after the 3 days TOS period. Similar data over each of the 3 day operating periods for the other catalysts show the same trend (Tables S3−S7, Supporting Information). As there was some deactivation of the catalyst during the 3 day period, all comparisons have been made after a TOS period of 3 days. These data comparisons follow the same approach reported by Alzaid et al. for a commercial NiMoS/γ-Al_2O_3 catalyst.[16] The products of the reaction, indicative of both hydrogenation and dimerization reactions, were similar to those reported by Alzaid et al.,[16] except for the ~10 wt % yield of 1-ethyl-4-methyl cyclohexane, at a higher reaction temperature (250 °C), which was absent from the products of this study obtained at 200 °C.

Figure 2 compares the total acidity among the various catalysts (from Table 1) and the corresponding C_{18} dimer yield

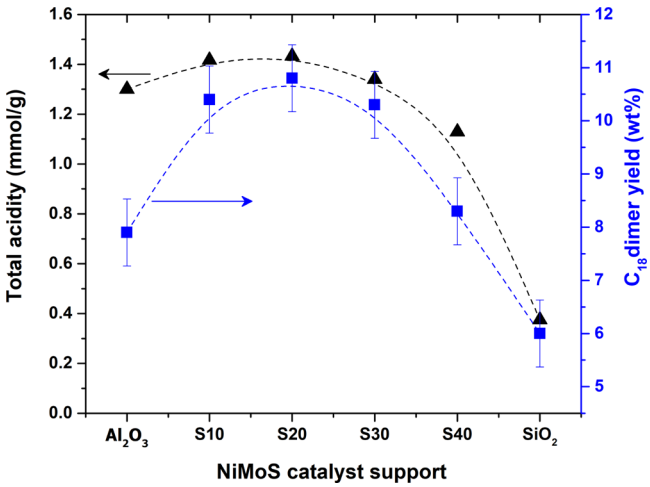

Figure 2. C_{18} yield and total acidity of NiMoS catalysts on different supports. Dimer yield measured at 200 °C, 3.4 MPa H_2, LHSV = 4 h^{-1}, H_2/feed = 392 mL(STP)/mL, with 8.4 wt % 4-MS in decalin, and TOS of 3 days (dotted line to guide the eye).

measured at 200 °C, 3.4 MPa H_2, and LHSV = 4 h^{-1} with 8.4 wt % 4-MS in decalin after the 3 days TOS period. Clearly, the dimer yield is related to the total acidity of the catalyst. The NiMoS/S10 and NiMoS/S20 catalysts, with the highest acidity, had the highest C_{18} dimer yield, whereas, NiMoS/SiO_2 had the lowest acidity and a correspondingly lower C_{18} dimer yield. To distinguish which type of acidity is responsible for the dimer yield, the C_{18} dimer yield was also plotted as a function of the Lewis and Brønsted acidities, respectively (see Figure S5, Supporting Information). Although the plots show similar correlations, the dominance of Lewis acidity on these catalysts means that it is not possible to distinguish between the significance of Lewis versus Brønsted acidity. Hence, we conclude that the correlations between the dimer yield, total acidity, Lewis acidity, and Brønsted acidity are very similar, with a maximum C_{18} dimer yield reported for the NiMoS/S20 catalyst, corresponding to the highest total acidity (and highest Lewis and Brønsted acidities). Note that the dimerization of 4-MS can occur on both Brønsted and Lewis acid sites. The yield data of Figure 2 corresponding to the NiMoS/SiO_2 catalyst may also be influenced by the relatively small pore diameter of this catalyst (2.9 nm). However, potential internal diffusion effects were minimized by the use of a small catalyst particle size (1.41 mm).[28] Furthermore, the kinetic diameters of 4-MS (~0.6 nm) and the product dimer are much less than the NiMoS/SiO_2 catalyst pore diameter, suggesting that the yield data would not be significantly influenced by internal diffusion effects.[28]

Table S8 compares the product yields after the 3 days TOS period for the catalysts, showing that as the SiO_2 content of the SiO_2−Al_2O_3 support increased, corresponding to a decrease in acidity, the yield of 1-ethyl-4-methyl-benzene and 1,3-di(4′-methylphenyl)butane decreased. The catalyst with the lowest acidity (NiMoS/SiO_2) had the lowest yield of both 1-ethyl-4-methyl-benzene and dimers at the chosen operating conditions. The intermediate dimer 1,3-di-(4′methylphenyl) butene had a low yield (~0.5 wt %) among all the catalysts as it was readily hydrogenated to yield 1, 3-di(4′-methylphenyl) butane. Finally, the ring-opening dimer (1,1-dimethyl decyl)-benzene was detected with a yield of ~0.4 wt % on all the catalysts.

The data reported herein were obtained at a high conversion of 4-MS, as required in industrial operations. However, in a previous work, Alzaid[28] showed that the dimer yield increased at lower conversions of 4-MS (i.e., increased LHSV). In addition, Alzaid et al.[16] reported that at a lower reaction temperature, a faster decrease in conversion with TOS was detected, accompanied by a higher yield of dimers. These trends were attributed to higher concentrations of 4-MS that enhanced the dimerization reaction rate more than the hydrogenation rate. In the present study, 4-MS conversion was significantly lower on the NiMoS/SiO_2 catalyst compared to the NiMoS/SiO_2−Al_2O_3 catalysts (Tables S2−S7). At higher conversions, the dimer yield on the NiMoS/SiO_2 catalyst would be expected to decrease. Hence, comparing the catalysts at the same 4-MS conversion would tend to magnify the correlation reported in Figure 2 that shows increased dimer yield with increased acidity.

To distinguish between the dimerization from acid sites located on the support versus those associated with NiMoS, the sulfided supports alone (without NiMoS) were also used as catalysts and operated at the same reaction conditions as with the supported NiMoS catalysts. As shown in Table S9 for the S10−S sulfided support, 4-MS was also converted to the hydrogenation product 1-ethyl-4-methyl-benzene and C_{18} dimers. However, the hydrogenated product yield decreased significantly over the 3 day period from 76.1 to 6.1 wt %, likely because of the lack of NiMoS hydrogenation sites on the catalyst. The main C_{18} dimer over the support was 1,3-di-(4′-methylphenyl) butane, the same as that for the NiMoS catalysts on the same support (Table S8), with a ~3.5 wt % yield and a total C_{18} product yield of ~3.8 wt % after the 3 days TOS period. Similar data over each of the 3 days for the other supports showed the same trend (Tables S9−S14, Supporting Information).

The relationship between the total acidity of the sulfided support and the C_{18} dimer yield is reported in Figure 3. The

https://doi.org/10.1021/acs.energyfuels.1c00787
Energy Fuels 2021, 35, 10113−10121

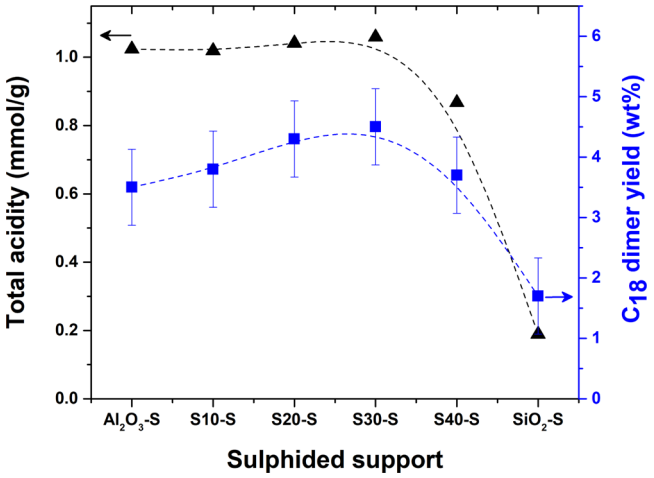

Figure 3. C_{18} yield related to the acidity of different sulfided supports (no NiMoS) at 200 °C, 3.4 MPa H_2, LHSV = 4 h^{-1}, and H_2/feed = 392 mL(STP)/mL, after 3 days of TOS period.

C_{18} dimer yield on the sulfided supports was about 40% of the value reported for the corresponding NiMoS-supported catalysts of Figure 2, and the yield data also correlated with the sulfided support acidity, as shown in Figure 3.

The total acidity data of Table 1 show that about 70% of the supported NiMoS catalyst acidity arises from the support. However, the data of Figures 2 and 3 indicate that the sulfided supports contribute about 40% of the total C_{18} dimerization yield obtained over the supported NiMoS catalysts. Hence, it is apparent that there is some synergistic effect on the dimerization reaction between the support and NiMoS, with the supported NiMoS catalysts having a higher yield of C_{18} dimers than that would be expected based only on the acidity of the catalyst.

An important difference in the stability of the supported NiMoS catalysts and the sulfided supports over the 3 day TOS period is captured in Figure 4. At the same aforementioned reaction conditions (8.4 wt % 4-MS reacted at 200 °C, 3.4 MPa H_2, LHSV = 4 h^{-1}, and H_2/feed = 392 mL(STP)/mL), the NiMoS/SiO_2−Al_2O_3 catalysts were relatively stable over the 3 day TOS period as the 4-MS conversion remained high (>90%). The NiMoS/SiO_2 catalyst was less stable with the 4-MS conversion decreasing from 68 to 42% over the 3 day period. However, all the sulfided supports (no NiMoS) deactivated significantly over the 3 day TOS period, as shown in Figure 4B. Although S10−S, S20−S, S30−S, and S40−S showed very high 4-MS conversion on the first day, the conversions declined rapidly by the third day.

The yields of 1-ethyl-4-methyl-benzene and C_{18} products were also stable over the 3 day period on the NiMoS catalysts, as shown in Figure 5A,B. The hydrogenation of 4-MS over the different NiMoS catalysts followed the same stability trend as 4-MS conversion, shown in Figure 4A, as the hydrogenation of 4-MS was the major reaction at all conditions investigated. Figure 5C,D also shows that the yield of 1-ethyl-4-methyl-benzene and C_{18} products on the sulfided supports declined with TOS, with the decline in the hydrogenation product yield significantly faster than the decline in the dimer yield. Clearly, the presence of NiMoS resulted in an improved catalyst stability due to the ability to hydrogenate more of the olefins and reduce the dimerization and ultimately gum formation that blocks the catalyst active sites.

The hydrogenation reactions on the sulfided support occur via a hydride transfer reaction mechanism involving the solvent decalin, as has been reported previously.[35−37] As shown in Figure S6, if 4-MS binds on an acid site and is protonated to form the corresponding carbocation of 4-MS, a free decalin molecule can transfer a hydride ion to the protonated 4-MS, resulting in 1-ethyl-4-methyl-benzene (note that Figure S6 assumes protonation on a Brønsted acid site, but an equivalent sequence can be written for the Lewis site as well). Finally, the protonated decalin donates a proton (proton cycle) and forms 1,2,3,4,4a,5,8,8a-octahydronaphthalene. The hydride transfer process is presumably much slower than the dimerization of the protonated 4-MS, resulting in a rapid deactivation of the catalysts as 4-MS dimerizes faster. Similar deactivation trends were observed for Al_2O_3−S and SiO_2−S. The 4-MS conversion on SiO_2−S was low, consistent with the low acidity of this support. However, a similar low conversion on Al_2O_3−S, despite a high acidity, indicates that the Lewis acid sites present on the sulfided SiO_2−Al_2O_3 supports are different to those on Al_2O_3−S.

The data of Figures 4 and 5 indicate that hydrogenation of the conjugated olefin 4-MS occurs on active sites associated with the NiMoS phase, in agreement with previous studies that have shown that hydrogenation reactions occur on the edge sites of the NiMoS slabs present on the catalyst. On the other

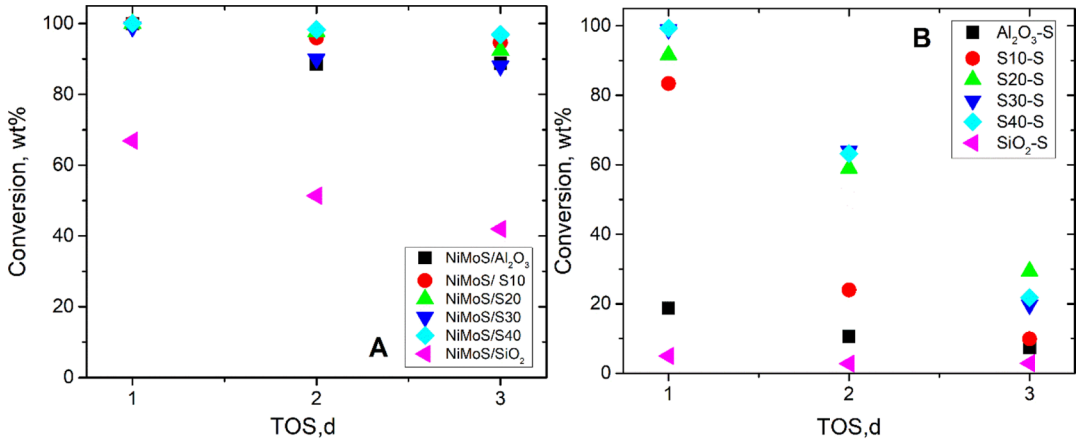

Figure 4. 4-MS conversion with TOS of different NiMoS/SiO_2−Al_2O_3 catalysts (A) and SiO_2−Al_2O_3-sulfided supports (B) using 8.4 wt % 4-MS at 200 °C, 3.4 MPa H_2, LHSV = 4 h^{-1}, and H_2/feed = 392 mL(STP)/mL.

https://doi.org/10.1021/acs.energyfuels.1c00787
Energy Fuels 2021, 35, 10113−10121

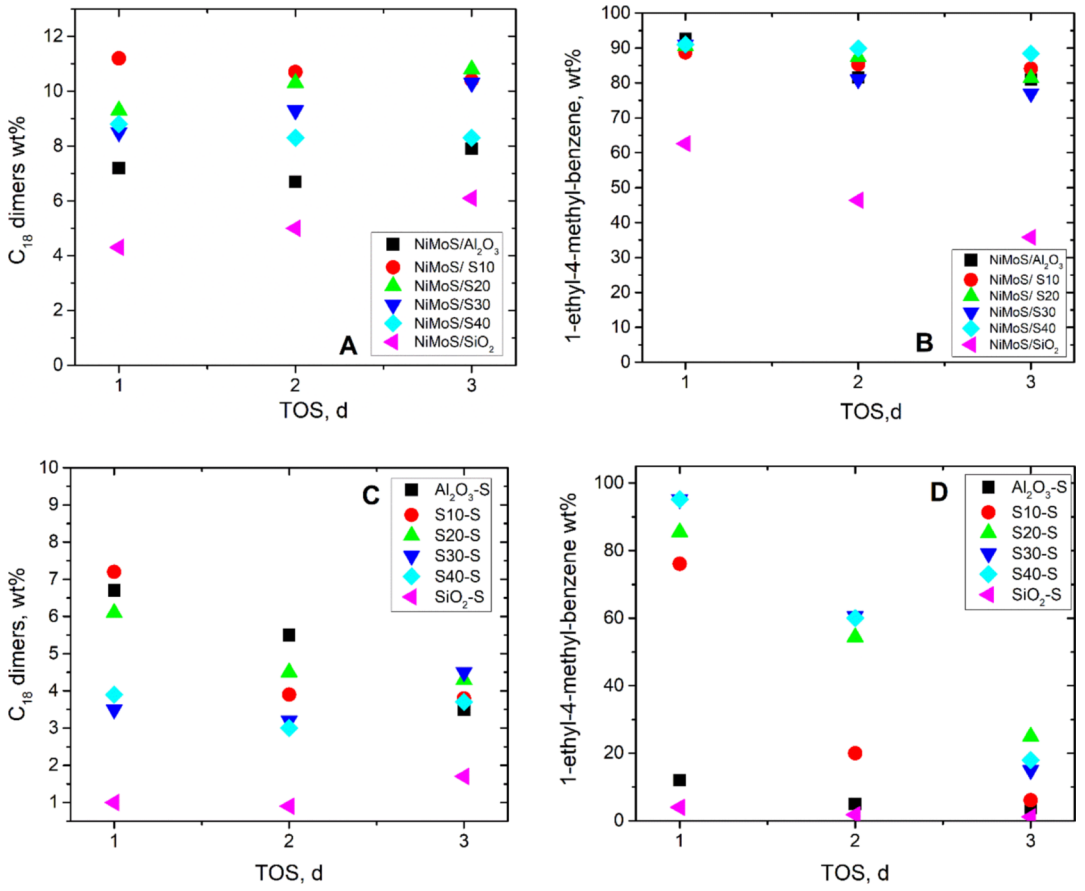

Figure 5. Product selectivity with TOS during 4-MS hydrogenation on $NiMoS/SiO_2-Al_2O_3$ catalysts (A,B) and the sulfided $SiO_2-Al_2O_3$ supports (C,D) using 8.4 wt % 4-MS at 200 °C, 3.4 MPa H_2, LHSV = 4 h^{-1}, and H_2/feed = 392 mL(STP)/mL.

hand, the acid sites result in relatively constant dimerization yields, and we provide evidence that the acidity of the support and the NiMoS phase can contribute to the dimerization. We also report that in the presence of NiMoS, the dimerization yield increased, indicating that the presence of NiMoS enhanced acidity and reduced the loss in active sites caused by the deposition of gum precursors.

Finally, we examined the impact of neutralizing some of the catalyst acidity by preparing a NiMoS/S10 catalyst doped with a NaOH base. The catalyst was prepared by incipient wetness impregnation, sequentially doping the S10 support with 8 wt % Mo, 2 wt % Ni, and 3 wt % Na (from a 50% NaOH solution, Sigma-Aldrich). The catalyst was presulfided, following the same procedure as before. The acidity of neutralized NiMoS/S10 (3 wt % Na), measured by NH_3TPD, decreased by about 60% compared to NiMoS/S10, as shown in Table 3.

As about 70% of the NiMoS/S10 acidity was contributed by the support (Table 1), NaOH must have neutralized a substantial portion of the support acid sites. However, Figure 6A shows that despite the drop in acidity caused by the NaOH neutralization, the conversion of 4-MS was unchanged, suggesting that the NaOH dopant did not negatively impact

Table 3. NH_3 TPD Measurement for NiMoS/S10 Versus NiMoS/S10 (3 wt % Na)

catalysts	acidity (mmol/g)
NiMoS/S10	1.42
NiMoS/S10 Na (3 wt %)	0.60

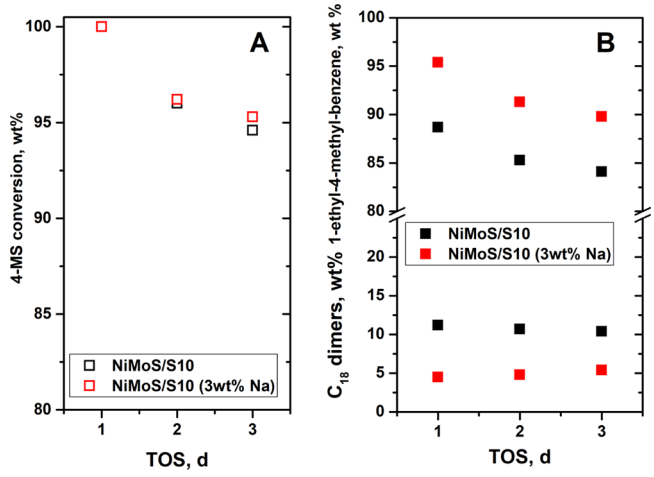

Figure 6. 4-MS conversion (A) and yield of the main hydrogenated product and C_{18} dimers (B) with NiMoS/S10 and NiMoS/S10 (3 wt % Na) catalysts and 8.4 wt % 4-MS reacted at 200 °C, 3.4 MPa H_2, LHSV = 4 h^{-1}, and H_2/feed = 392 mL(STP).

the hydrogenation active sites of the catalyst, which are assumed to be associated with the NiMoS phase. Figure 6B shows a 50−60% decrease in the dimer yield (with a corresponding increase in the hydrogenation product yield) following NaOH treatment, suggesting that NaOH was most effective in neutralizing the acid sites associated with the support, while maintaining the conversion to the hydrogenated products. These results suggest that the catalyst life span could

https://doi.org/10.1021/acs.energyfuels.1c00787
Energy Fuels 2021, 35, 10113−10121

be prolonged by neutralizing the acid sites of the support as the dimerization yield is significantly reduced.

CONCLUSIONS

The hydrogenation and dimerization of isoprene and 4-MS over NiMoS/SiO_2−Al_2O_3 catalysts have been studied under conditions relevant to the low-temperature hydrogenation of Canadian oil sands naphtha. The acidity of the catalysts played a significant role in the production of dimers that lead to reactor fouling. The yield of C_{18} dimers produced during 4-MS hydrogenation at 200 °C, 3.4 MPa H_2, LHSV = 4 h^{-1}, and H_2/feed = 392 mL(STP)/mL correlated with the total acidity of the catalysts. The NiMoS catalysts had high yields of hydrogenation products (>80%), whereas the sulfided supports deactivated rapidly. The higher yield of dimers in the presence of the NiMoS/SiO_2−Al_2O_3 catalyst compared to the support alone can only be partly attributed to the higher acidity of the NiMoS/SiO_2−Al_2O_3 catalysts. Higher-than-expected dimer yields are thought to arise because of the synergistic effects between the hydrogenation sites and acid sites of the catalyst, which decrease the deactivation of acid sites by gum deposition. Neutralizing the catalysts with NaOH showed a promising result with ∼50% reduction in dimerization yield.

ASSOCIATED CONTENT

Supporting Information

The Supporting Information is available free of charge at https://pubs.acs.org/doi/10.1021/acs.energyfuels.1c00787.

NH_3 TPD temperature profiles for NiMoS catalysts on different supports; NH_3 TPD temperature profiles for different sulfided supports; DRIFT spectra for NiMoS/SiO_2−Al_2O_3 and HRTEM images; C_{18} yield related to the Lewis and Brønsted acidities of different catalysts; reaction steps for the hydrogenation of 4-MS by hydride transfer from decalin; product yield data from delayed coke and fluid coke processing of Alberta bitumen; and product yield data and conversions for 4-MS on various catalysts and catalyst supports as a function of TOS (PDF)

AUTHOR INFORMATION

Corresponding Author

Kevin J. Smith − *Department of Chemical and Biological Engineering, University of British Columbia, Vancouver, British Columbia V6T 1Z3, Canada;* orcid.org/0000-0001-6008-0223; Phone: +1 604-822-3601; Email: kjs@mail.ubc.ca

Authors

Majed A. Alamoudi − *Department of Chemical and Biological Engineering, University of British Columbia, Vancouver, British Columbia V6T 1Z3, Canada; Department of Chemical and Materials Engineering, Faculty of Engineering, King Abdulaziz University, Jeddah 21589, Saudi Arabia*

Hamad Almohamadi − *Department of Chemical Engineering, Faculty of Engineering, Islamic University of Madinah, Madinah 42351, Saudi Arabia*

Complete contact information is available at: https://pubs.acs.org/10.1021/acs.energyfuels.1c00787

Notes

The authors declare no competing financial interest.

ACKNOWLEDGMENTS

The financial support of the Natural Sciences and Engineering Research Council of Canada (NSERC) is gratefully acknowledged. MA acknowledges scholarship support from King Abdulaziz University, Jeddah, Saudi Arabia.

ABBREVIATION

ASA = amorphous aluminosilicates
BET = Brunauer−Emmett−Teller
CUS = coordinatively unsaturated sites
EDX = energy-dispersive X-ray
f_{Mo} = MoS_2 dispersion
GC−MS = gas chromatography−mass spectrometry
HDS = hydrodesulfurization
HRTEM = high-resolution transmission electron microscopy
HYDO = hydrogenation
HAADF = high-angle annular dark field
L_i = the length of the layers of MoS_2 crystallites
LHSV = liquid hourly space velocity
MCT = mercury cadmium telluride
4-MS = 4-methylstyrene
n_i = number of edge-site Mo atoms of a single layer
N_i = the number of layers of each crystallite
NH_3TPD = ammonia temperature-programmed desorption
Py-DRIFT = pyridine-adsorbed diffuse reflectance infrared Fourier transform
TOS = time on stream
x = total number of crystallites observed in the micrographs

REFERENCES

(1) Government of Canada. Crude oil facts. https://www.nrcan.gc.ca/science-data/data-analysis/energy-data-analysis/energy-facts/crude-oil-facts/20064 (accessed Nov 20, 2020).
(2) Gray, M.; Xu, Z.; Masliyah, J. Physics in the oil sands of alberta. *Phys. Today* **2009**, *62*, 31−35.
(3) Chevron Lummus Global, LC-fining. http://www.cbi.com (accessed Feb 21, 2017).
(4) Gray, M. R. Thermal and Coking Processes. *Upgrading Petroleum Residues and Heavy Oils*: CRC Press: New York, 1994; pp 237−259.
(5) Yui, S. Removing diolefins from coker naphtha necessary before hydrotreating. *Oil Gas J.* **1999**, *97*, 64.
(6) Sales, E. A.; de Jesus Mendes, M.; Bozon-Verduraz, F. Liquid-phase selective hydrogenation of hexa-1,5-diene and hexa-1,3-diene on palladium catalysts. effect of tin and silver addition. *J. Catal.* **2000**, *195*, 96−105.
(7) Dobrovolná, Z.; Kačer, P.; Červený, L. Competitive hydrogenation in alkene-alkyne-diene systems with palladium and platinum catalysts1This work is a part of the Selective Catalytic Hydrogenation and Transfer Hydrogenation project GA CR 104/96/1445.1. *J. Mol. Catal. A: Chem.* **1998**, *130*, 279−284.
(8) Wells, P. B.; Bates, A. J. The hydrogenation of alkadienes, Part II. The hydrogenation of buta-1,3-diene catalysed by rhodium, palladium, iridium, and platinum wires. *J. Chem. Soc. A* **1968**, 3064−3069.
(9) Goetz, J.; Murzin, D. Y.; Touroude, R. A. Kinetic Aspects of Selectivity and Stereoselectivity for the Hydrogenation of Buta-1,3-diene over a Palladium Catalyst. *Ind. Eng. Chem. Res.* **1996**, *35*, 703−711.
(10) Okuhara, T.; Itoh, H.; Miyahara, K.; Tanaka, K. Hydrogenation of dienes and the selectivity for partial hydrogenation on a molybdenum disulfide catalyst. *J. Phys. Chem.* **1978**, *82*, 678−682.
(11) The European parliament and the council of the european union, directive 2009/30/EC. http://eur-lex.europa.eu/legal-content/EN/TXT/?uri=celex%3A32009L0030 (accessed Feb 22, 2021).

(12) Bartholomew, C. H.; Farrauto, R. J. Introduction and fundamentals. *Fundamentals of industrial catalytic processes*; John Wiley & Sons, Inc., 2005; pp 3−59.
(13) Wambeke, A.; Jalowiecki, L.; Kasztelan, S.; Grimblot, J.; Bonnelle, J. P. The active site for isoprene hydrogenation on MoS_2/γ-Al_2O_3 catalysts. *J. Catal.* **1988**, *109*, 320−328.
(14) Jalowiecki, L.; Aboulaz, A.; Kasztelan, S.; Grimblot, J.; Bonnelle, J. P. Hydrogenation and isomerization of alkadienes on powdered MoS_xH_y. *J. Catal.* **1989**, *120*, 108−117.
(15) Alzaid, A.; Wiens, J.; Adjaye, J.; Smith, K. J. Impact of molecular structure on the hydrogenation and oligomerization of diolefins over a Ni-Mo-S/γ-Al_2O_3 catalyst. *Fuel* **2018**, *221*, 206−215.
(16) Alzaid, A.; Wiens, J.; Adjaye, J.; Smith, K. J. Catalyst deactivation and reactor fouling during hydrogenation of conjugated cyclic olefins over a commercial Ni−Mo−S/γ-Al_2O_3 catalyst. *Energy Fuels* **2018**, *32*, 6213−6223.
(17) de la Puente, G.; Sedran, U. Formation of gum precursors in fcc naphthas. *Energy Fuels* **2004**, *18*, 460−464.
(18) Gates, B. C.; Katzer, J. R.; Schuit, G. C. Cracking. *Chemistry of catalytic processes*; McGraw-Hill: New York, 1979; Vol. *464*; pp 42−49.
(19) Naccache, C. Deactivation of acid catalysts. In *Deactivation and Poisoning of Catalysts*; Oudar, J., Wise, H., Eds.; CRC Press: New York, 1985; Vol. *20*; pp 185−197.
(20) Pradelle, F.; Braga, S. L.; Martins, A. R. F. A.; Turkovics, F.; Pradelle, R. N. C. Gum formation in gasoline and its blends: A review. *Energy Fuels* **2015**, *29*, 7753−7770.
(21) Uzcátegui, G.; Fong, S. Y.; de Klerk, A. Cracked naphtha reactivity: Effect of free radical reactions. *Energy Fuels* **2018**, *32*, 5812−5823.
(22) Weissman, J. G.; Edwards, J. C. Characterization and aging of hydrotreating catalysts exposed to industrial processing conditions. *Appl. Catal., A* **1996**, *142*, 289−314.
(23) de Klerk, A. Oligomerization of 1-hexene and 1-octene over solid acid catalysts. *Ind. Eng. Chem. Res.* **2005**, *44*, 3887−3893.
(24) Quann, R. J.; Green, L. A.; Tabak, S. A.; Krambeck, F. J. Chemistry of olefin oligomerization over ZSM-5 catalyst. *Ind. Eng. Chem. Res.* **1988**, *27*, 565−570.
(25) Pérez-Martínez, D. J.; Gaigneaux, E. M.; Giraldo, S. A.; Centeno, A. Interpretation of the catalytic functionalities of CoMo/ASA FCC-naphtha-HDT catalysts based on its acid properties. *J. Mol. Catal. A: Chem.* **2011**, *335*, 112−120.
(26) Yang, S. H.; Satterfield, C. N. Catalytic hydrodenitrogenation of quinoline in a trickle-bed reactor. effect of hydrogen sulfide. *Ind. Eng. Chem. Process Des. Dev.* **1984**, *23*, 20−25.
(27) Corma, A.; Martinez, A. Zeolites and zeotypes as catalysts. *Adv. Mater.* **1995**, *7*, 137−144.
(28) Alzaid, A. H. Impact of Conjugated Olefins on Ni-Mo-S/γ-Al2O3 Catalyst Deactivation and Fouling of Naphtha Hydrotreaters. Ph.D. Thesis, University of British Columbia: Vancouver, Canada, 2016.
(29) Kasztelan, S.; Toulhoat, H.; Grimblot, J.; Bonnelle, J. P. A geometrical model of the active phase of hydrotreating catalysts. *Appl. Catal.* **1984**, *13*, 127−159.
(30) Tye, C. T.; Smith, K. J. Catalytic activity of exfoliated MoS_2 in hydrodesulfurization, hydrodenitrogenation and hydrogenation reactions. *Top. Catal.* **2006**, *37*, 129−135.
(31) Tye, C. T.; Smith, K. J. Hydrodesulfurization of dibenzothiophene over exfoliated MoS_2 catalyst. *Catal. Today* **2006**, *116*, 461−468.
(32) Hensen, E. J. M.; Kooyman, P. J.; van der Meer, Y.; et al. The relation between morphology and hydrotreating activity for supported MoS_2 particles. *J. Catal.* **2001**, *199*, 224−235.
(33) Daniell, W.; Schubert, U.; Glöckler, R.; Meyer, A.; Noweck, K.; Knözinger, H. Enhanced surface acidity in mixed alumina-silicas: a low-temperature FTIR study. *General* **2000**, *196*, 247−260.
(34) Lenarda, M.; Da Ros, M.; Casagrande, M.; Storaro, L.; Ganzerla, R. Post-synthetic thermal and chemical treatments of H-BEA zeolite: Effects on the catalytic activity. *Inorg. Chim. Acta* **2003**, *349*, 195−202.
(35) Alemán-Vázquez, L. O.; Cano-Domínguez, J. L.; García-Gutiérrez, J. L. Effect of tetralin, decalin and naphthalene as hydrogen donors in the upgrading of heavy oils. *Procedia Eng.* **2012**, *42*, 532−539.
(36) Obara, T.; Yokono, T.; Sanada, Y. Relationships between hydrogen donor abilities and chemical structure of aromatic compounds in terms of coal liquefaction. *Fuel* **1983**, *62*, 813−816.
(37) Cronauer, D. C.; Jewell, D. M.; Shah, Y. T.; Modi, R. J. Mechanism and kinetics of selected hydrogen transfer reactions typical of coal liquefaction. *Ind. Eng. Chem. Fundam.* **1979**, *18*, 153−162.

https://doi.org/10.1021/acs.energyfuels.1c00787
Energy Fuels 2021, 35, 10113−10121